SEECCM III
3rd South-East European Conference on Computational Mechanics-
an ECCOMAS and IACM Special Interest Conference
M. Papadrakakis, M. Kojic, I. Tuncer (eds.)
Kos Island, Greece, 12–14 June 2013

BLOOD FLOW SIMULATION IN THE AORTA PASSING THROUGH THE AORTIC ORIFICE BY VIRTUAL FLUX METHOD

T. Fukui[1] **and K. Morinishi**[2]

[1] Department of Mechanical and System Engineering, Kyoto Institute of Technology
Gosyokaido-cho, Matsugasaki, Sakyo-ku, Kyoto 606-8585, Japan
e-mail: fukui@kit.ac.jp

[2] Department of Mechanical and System Engineering, Kyoto Institute of Technology
Gosyokaido-cho, Matsugasaki, Sakyo-ku, Kyoto 606-8585, Japan
e-mail: morinisi@kit.ac.jp

Keywords: Aortic Valves, Sinus of Valsalva, Vorticity, Wall Shear Stress, Virtual Flux Method, Regularized Lattice Boltzmann Method, Multi-block Method.

Abstract. *Transposition of the great arteries (TGA) is one of the most severe congenital heart disease. The arterial switch operation (ASO) is the procedure of preference for treatment of TGA. After ASO, some patients suffer from circulatory system problems such as neo-aortic root dilatation and neo-aortic valve regurgitation, and supravalvar pulmonary stenosis. The neo-aortic root dilatation is often explained by the structural vascular difference between normal great arteries and the neo-aorta after ASO. Since the aortic and pulmonary roots generally remain in situ after ASO, i.e., the original pulmonary artery is connected to the left ventricle (LV), whereas the original aorta is connected to the right ventricle, the neo-aorta has no sinus of Valsalva after ASO. The influence of these morphological changes on the blood flow field at the aortic root should be investigated in detail as well as the structural vascular difference to consider the circular system problems. In this study, we apply the virtual flux method (VFM), which is a tool to describe stationary or moving body shapes in a Cartesian grid, to the 2D aortic valves with a multi-block method for high resolution near the valves, and reproduce the blood flow fields around the aortic valves and the sinus of Valsalva by RLBM, and consider the influence of longitudinal length of sinus of Valsalva on blood flow fields around the aortic valves. As a result, we found that the longitudinal length of the sinus affects development of vortices around the aortic valves strongly. We also found that the WSS increases toward the distal edge of the sinus, indicating the WSS value at the distal edge of the sinus is dependent on the longitudinal length of the sinus of Valsalva.*

1 INTRODUCTION

Transposition of the great arteries (TGA) is one of the most severe congenital heart disease. Since the aorta arises from the right ventricle in TGA, blood in the systemic circulation is always rich in carbon dioxide and poor in oxygen. On the other hand, the pulmonary circulation in TGA is always full of blood with oxygen. The systemic and pulmonary circulations are completely separated in TGA. The arterial switch operation (ASO) is the procedure of preference for treatment of TGA. Although many reports have shown good results after ASO [1,2,3], some patients suffer from circulatory system problems such as neo-aortic root dilatation and neo-aortic valve regurgitation [4,5], and supravalvar pulmonary stenosis [6] after ASO. Diameters of aortic annulus and sinus of Valsalva 20 years after ASO are significantly wider in comparison to a normal population of young adults, whereas ascending aorta diameters are well preserved in our population and are not significantly different to the values in a normal population, demonstrating that dilatation of the aortic root is due to a localized problem [7]. This localized dilatation of the aortic root is often explained by the structural vascular difference between normal great arteries and the neo-aorta after ASO [8].

Fluid dynamic forces against the arterial wall should be considered as well as the structural difference. The morphology of the aorta and aortic valves movement strongly affect the blood flow fields in the aorta, especially at the root of the aorta. In addition, the sinus of Valsalva, which lies at the aortic root, plays an important role for aortic valves behavior [9]. Since the aortic and pulmonary roots generally remain in situ after ASO, i.e., the original pulmonary artery is connected to the left ventricle (LV), whereas the original aorta is connected to the right ventricle, the neo-aorta has no sinus of Valsalva after ASO. Moreover, there are some cases that the curvature of the neo-aortic root is extremely larger than that in a normal population due to ASO. The influence of these morphological changes on the blood flow field at the aortic root should be investigated in detail.

In the past study, we performed numerical simulation of blood flows around aortic valves by lattice Boltzmann method [10,11]. The method of lattice Boltzmann equation (LBM) is a simple kinetic-based approach for fluid flow computation. The LBM has advantages its simple coding and its locality, which makes it intrinsically parallelizable [12], and has been applied to many problems relevant to blood flow simulation [13,14,15]. However, stability of the simulation by LBM is strictly dependent on its relaxation time, which leads to restriction of the Reynolds number. Since blood flow simulation in the aorta is accompanied by high Reynolds number, it is necessary to improve stability of LBE. Izham et al. [16] proposed regularized lattice Boltzmann method (RLBM), which is based on the observation of symmetric condition in Chapman-Enskog expansion by Latt & Chopard [17], and it has successfully achieved higher stability in numerical simulation at high Reynolds number. In this study, we apply the virtual flux method (VFM) [18], which is a tool to describe stationary or moving body shapes in a Cartesian grid, to the 2D aortic valves with a multi-block method [19,20] for high resolution near the valves, and reproduce the blood flow fields around the aortic valves and the sinus of Valsalva by RLBM, and consider the influence of longitudinal length of sinus of Valsalva on blood flow fields around the aortic valves.

2 METHODS

2.1 Computational models

Numerical simulation of blood flow in aorta with valves and sinus of Valsalva is performed. Figure 1 shows the schematic view of the 2-dimensional axisymmetric simulation model used in this study. The longitudinal length L and diameter D are set to 200 mm and 20 mm. The valve leaflets are modeled as arcs of a circle with a radius of $D/\sqrt{2}$, and placed at 80 mm (= 4D) from the inlet. The shape of the sinus of Valsalva is approximated as a semi-ellipse. The longitudinal length a and depth b of the sinus of Valsalva are set to a = 30 mm and b = 15 mm for case 1, and a = 40 mm and b = 15 mm for case 2, respectively. The arterial wall and valves are described by virtual flux method on Cartesian coordinate as described below.

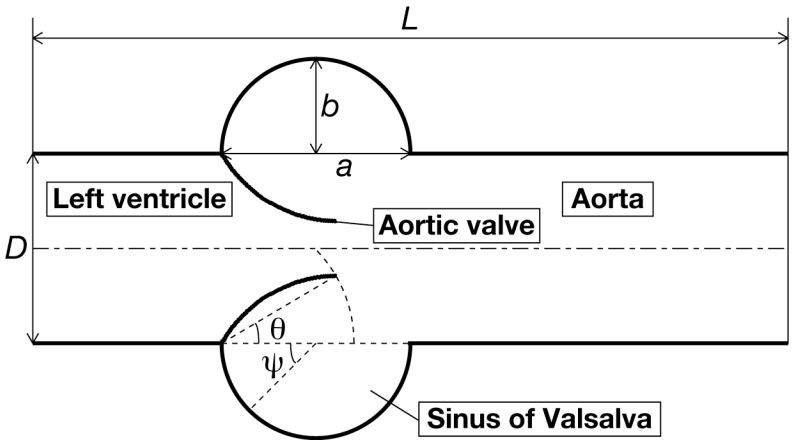

Figure 1: Schematic view of the computational model.

2.2 Governing equations

The discrete velocity Boltzmann equation (DVBE) is as follows,

$$\frac{\partial f_\alpha}{\partial t} + \boldsymbol{e}_\alpha \cdot \nabla f_\alpha = \boldsymbol{\Omega}_\alpha, \tag{1}$$

where $\boldsymbol{e}_\alpha$ is the discrete particle velocity, f_α is the distribution function associated with $\boldsymbol{e}_\alpha$, and $\boldsymbol{\Omega}_\alpha$ is the collision operator. The collision operator, which is very complicated, is usually approximated by the simple single-relaxation-time Bhatnagar-Gross-Krook (BGK) model [21]:

$$\boldsymbol{\Omega}_\alpha = -\frac{1}{\tau}\left(f_\alpha - f_\alpha^{(eq)}\right), \tag{2}$$

where $f_\alpha^{(eq)}$ is the equilibrium distribution function, and τ is the relaxation time. The evolution of the distribution function f_α for the lattice Boltzmann equation (LBE) can be written as

$$f_\alpha\left(\boldsymbol{x} + \boldsymbol{e}_\alpha \Delta t, t + \Delta t\right) - f_\alpha\left(\boldsymbol{x}, t\right) = -\frac{1}{\tau}\left\{f_\alpha\left(\boldsymbol{x}, t\right) - f_\alpha^{(eq)}\left(\boldsymbol{x}, t\right)\right\}. \tag{3}$$

In this study, we use a 2D square lattice model with 9 velocities, which is referred to as the D2Q9 model. It is shown that the Navier-Stokes equations can be derived from the LBE though a Chapman-Enskog expansion procedure in the incompressible limit [22] with a relaxation time τ as

$$\tau = \frac{3\nu}{c\delta x} + \frac{\delta t}{2}. \tag{4}$$

The most common choice for the equilibrium distribution function $f_\alpha^{(eq)}$ is the truncated form of the Maxwell distribution, which is a very good approximation for small Mach numbers [23].

$$f_\alpha^{(eq)} = \omega_\alpha \rho \left[1 + \frac{3(\boldsymbol{e}_\alpha \cdot \boldsymbol{u})}{c^2} + \frac{9(\boldsymbol{e}_\alpha \cdot \boldsymbol{u})^2}{2c^4} - \frac{3\boldsymbol{u}^2}{2c^2} \right], \tag{5}$$

where ω_α is the weight coefficients.

The single-relaxation-time (SRT) LBM has been widely used for its simplicity, efficiency and ease of parallel programming implementation, however, it requires relatively large number of grids to simulate flows at even moderately high Reynolds number. In Chapman-Enskog expansion procedure, the non-equilibrium part of first-order is symmetrical with respect to spatial reflection. Latt et al. [17] observed that this symmetric condition is not necessarily satisfied and appear to take a non-negligible value in numerical simulations using SRT-LBM. Based on this observation, they considered a regularization step that enforces symmetrical property and proposed regularized lattice Boltzmann method (RLBM).

The relationships between stress tensor and distribution function in RLBM [16] is defined as

$$\Pi_{ij} = \sum_\alpha e_{\alpha i} e_{\alpha j} f_\alpha, \tag{6}$$

where Π_{ij} is the stress tensor. The non-equilibrium part of the distribution and stress tensor were given as

$$f_\alpha^{(neq)} = f_\alpha - f_\alpha^{(eq)}, \tag{7}$$

$$\Pi_{ij}^{(neq)} = \Pi_{ij} - \Pi_{ij}^{(eq)}. \tag{8}$$

From the Chapman-Enskog expansion, the non-equilibrium part of ε-order can be explicitly derived as below,

$$f_\alpha^{(neq)} \approx f_\alpha^1 = -\frac{\delta t}{c_s^2} \tau \omega_\alpha \mathbf{Q}_{\alpha ij} \partial_i \rho u_j, \tag{9}$$

$$\Pi_{ij}^{(neq)} \approx \sum_\alpha e_{\alpha i} e_{\alpha j} f_\alpha^1 = -\delta t c_s^2 \tau \left(\partial_i \rho u_j + \partial_j \rho u_i \right), \tag{10}$$

where $\mathbf{Q}_{\alpha ij}$ is defined as

$$\mathbf{Q}_{\alpha ij} = e_{\alpha i} e_{\alpha j} - c_s^2 \delta_{ij}, \tag{11}$$

where c_s is the sound speed, and f_α^1 is then written as

$$f_\alpha^1 = \frac{\omega_\alpha}{2c_s^4} \mathbf{Q}_{\alpha ij} \Pi_{ij}^{(neq)}. \tag{12}$$

By enforcing $f_\alpha^{(neq)} = f_\alpha^1$, the final form of the relaxation process can be written as

$$f_\alpha = f_\alpha^{(eq)} + \left(1 - \frac{1}{\tau} \right) f_\alpha^1. \tag{13}$$

The viscous stress tensor τ_{ij} can be evaluated using the non-equilibrium part of the distribution function [24] as

$$\tau_{ij} = \left(1 - \frac{1}{2\tau}\right) \sum_{\alpha} f_{\alpha}^{(neq)}(\boldsymbol{x},t) \left(e_{\alpha i} e_{\alpha j} - \frac{1}{D} \boldsymbol{e}_{\alpha} \cdot \boldsymbol{e}_{\alpha} \delta_{ij} \right). \tag{14}$$

The aortic valves are assumed to be rigid, and their motion obeys following rigid-body rotation

$$\boldsymbol{T} = I \frac{d\boldsymbol{\omega}}{dt}, \tag{15}$$

where $\boldsymbol{T}$ is the torque, I is the inertia moment, and $\boldsymbol{\omega}$ is the angular velocity of the valve. The torque $\boldsymbol{T}$ is evaluated by force differences between LV-facing and aortic-facing surfaces of the valve,

$$\boldsymbol{T} = \sum \left(\boldsymbol{f}^{\mathrm{Ao}} - \boldsymbol{f}^{\mathrm{LV}} \right) \cdot r, \tag{16}$$

where r is the radius of rotation. The forces acting on the valve are obtained by pressure p and viscous stress τ_{ii} as follows,

$$\boldsymbol{f} = \left(p + \tau_{ii} \right) \cdot dr. \tag{17}$$

The inertia moment of the valve I is estimated by assuming the density of the valve is equal to that of the blood. The angular velocity $\boldsymbol{\omega}$ is obtained by first-order Euler method.

$$\boldsymbol{\omega}(t + \Delta t) = \boldsymbol{\omega}(t) + \Delta t \frac{\boldsymbol{T}(t)}{I}. \tag{18}$$

2.3 Boundary conditions

The virtual flux method (VFM) enables us to estimate flow field around arbitrary body shapes properly in a Cartesian grid [18]. In this study, we apply the VFM to express arbitrary body shapes appropriately in case that boundary points are not located on the cell vertex. Figure 2 shows an example of virtual flux boundary, where the virtual boundary point b is placed between cell vertexes 1 and 3. When the distribution function at vertex 1 is obtained, the distribution function at vertex 3, which includes the effect of the virtual boundary, is necessary, and vice versa. The macroscopic quantities on the virtual boundary point b are then determined to satisfy the boundary conditions. No-slip condition on the boundary, for example, is attained to assume zero pressure gradient and zero velocity on the boundary.

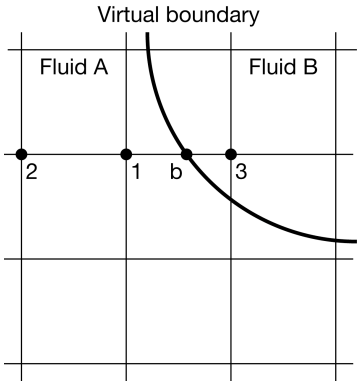

Figure 2: Schematic view of the virtual boundary in a Cartesian grid. The virtual boundary separates Fluid A from Fluid B completely.

Next, the equilibrium distribution function $p_\alpha^{(eq)}$ and distribution function p_α at the virtual boundary point b are obtained from the macroscopic quantities there. The distribution function p_α at the vertex 3 is then estimated to extrapolate that at the virtual boundary point b.

$$p_{\alpha,3} = \frac{p_{\alpha,\mathrm{b}} - (1-s)p_{\alpha,1}}{s}. \tag{19}$$

Axial velocity u at the inlet and pressure p at the outlet are given as shown in Fig. 3. Other parameters are linearly extrapolated. No-slip conditions are assumed on the wall and valve leaflets. The Reynolds number Re at the peak velocity in Fig. 3 corresponds to 2,000.

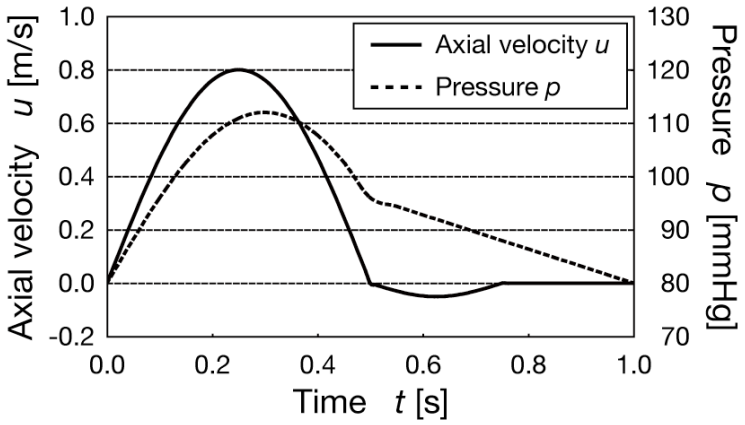

Figure 3: Axial velocity at the inlet and pressure at the outlet. The Reynolds number Re at the peak velocity corresponds to 2,000. The period of the cardiac cycle is set to 1.0 s

2.4 Multi-block method

A multi-block method [19,20] was used for high resolution near the aortic valves. Figure 4 illustrates the interface structure between two blocks of different lattice spacing. The ratio of the lattice space between the coarse and fine blocks is

$$m = \frac{\delta x_c}{\delta x_f}, \tag{20}$$

where δx_c and δx_f are the coarse and fine lattice sizes, respectively. In order to keep a consistent viscosity in the entire flow field involving different lattice sized, the relation between relaxation times τ_f on the fine grid and τ_c on the coarse grid must be obey the following rule:

$$\tau_f = \frac{1}{2} + m\left(\tau_c - \frac{1}{2}\right). \tag{21}$$

Since the velocity and density are continuous across the interface between the two blocks, the equilibrium part across the interface follows:

$$f_{\alpha,c}^{(eq)}(\boldsymbol{x},t) = f_{\alpha,f}^{(eq)}(\boldsymbol{x},t). \tag{22}$$

To maintain the continuity for the stress across the interface, the non-equilibrium part across the interface follows:

$$\left(1 - \frac{1}{2\tau_c}\right) f_{\alpha,c}^{(neq)}(\boldsymbol{x},t) = \left(1 - \frac{1}{2\tau_f}\right) f_{\alpha,f}^{(neq)}(\boldsymbol{x},t). \tag{23}$$

For the lattice Boltzmann method, in order to make sure that the interface uses information at the correct time level, three-point Lagrangian formulation is also used for the temporal interpolation at the interface.

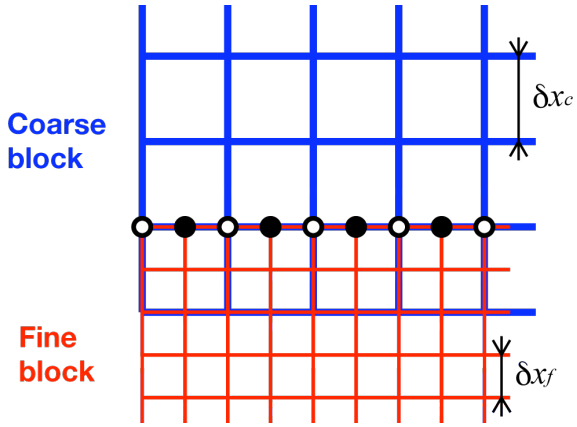

Figure 4: Interface structure between two blocks of different lattice spacing.

3 RESULTS AND DISCUTION

Figure 5 shows the vorticity distribution and velocity vectors on the left for case 1 and right for case 2 in the eighth cardiac cycle at the time interval of 0.1 s. When the pressure at the left ventricle (LV) exceeds that on the aorta, the valves start to open and blood flows toward the aorta passing through the aortic orifice. Vortices evolved from the tip of the valve spread and strike on the distal edge of the sinus of Valsalva, then they are divided into multiple (t = 0.3 ~ 0.4 s). This vortical motion has the advantage of preventing the valve leaflet from bulging outward to contact the walls of the sinuses. The vortices for case 2 are more dominant near the distal edge of the sinus, indicating that there needs an appropriate longitudinal length of the sinus for vortex development. These vortical motions then lead blood flow fields in the aorta to be more complicated. The open sinus chamber thus can be supplied with fluid to fill the increasing volume behind the valve leaflets as they move toward closure (t = 0.5 ~ 0.6 s). After the valves close the aortic orifice, multiple vortices do not completely dissipate in the aorta as well as in the sinus of Valsalva in diastole, so that they persist until the next systole. The aortic valve movements in systole have minor differences from cycle to cycle due to these vortices.

Figure 6 shows the time averaged wall shear stress (WSS) ratio τ_2 / τ_1 distribution on the LV-facing surface and aortic-facing surface of the aortic valves. The averaged WSS data in five cardiac cycles of case 2 τ_2 is divided by that of case 1 τ_1. The WSS ratio τ_2 / τ_1 on the LV-facing surface is relatively flat. On the other hand, the WSS ratio on the aortic-facing surface increases toward the tip of the valve. Figure 7 shows the time averaged WSS ratio distribution on the sinus wall in five cardiac cycles. The sinus position ψ = 0 and π rad correspond to proximal and distal edges of the sinus of Valsalva, respectively as shown in Fig. 1. The WSS ratio increases toward the distal edge of the sinus, indicating the WSS value at the distal edge of the sinus is dependent on the longitudinal length of the sinus of Valsalva.

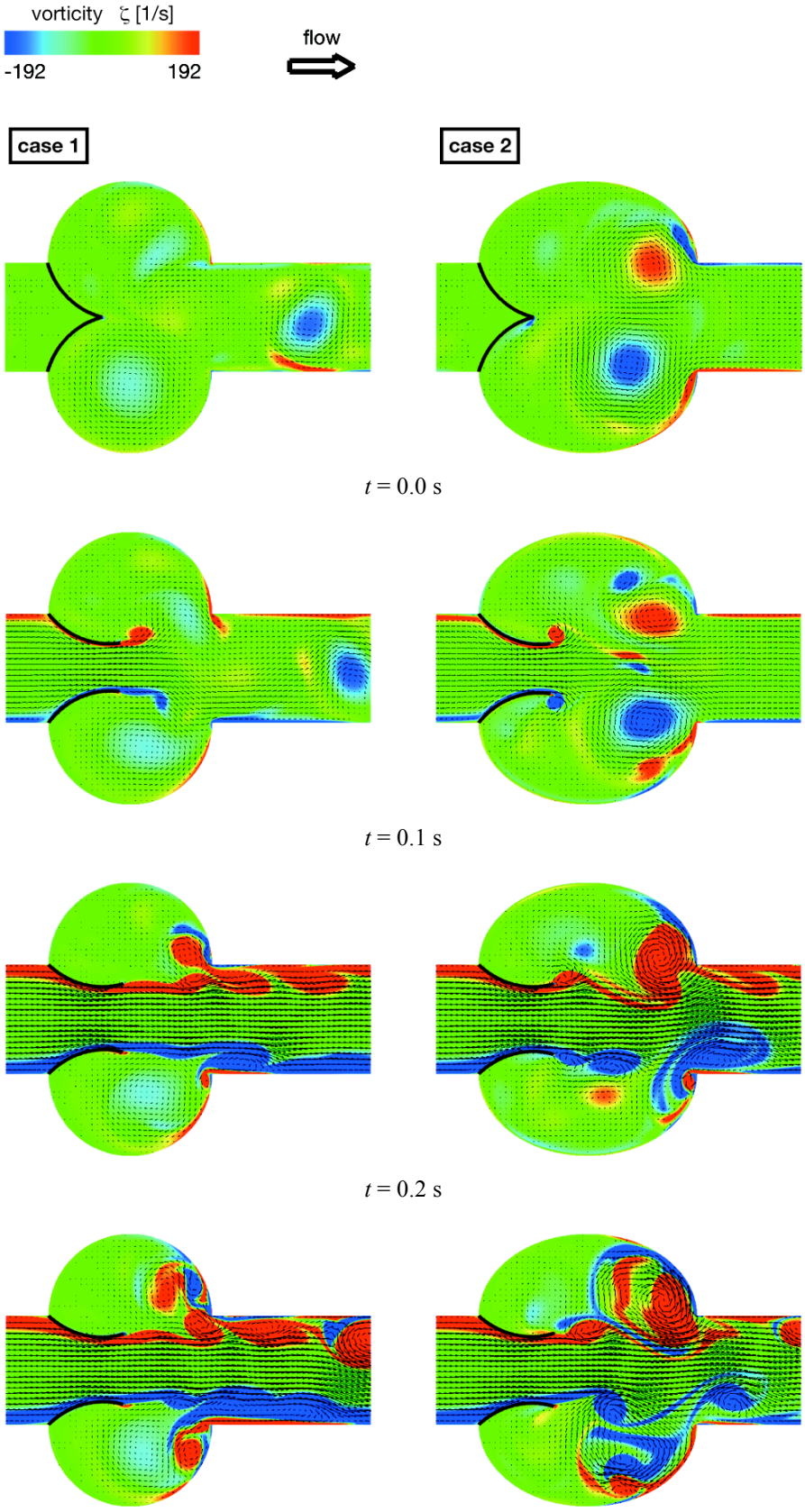
vorticity ζ [1/s]
-192
192
flow
case 1
case 2
t = 0.0 s
t = 0.1 s
t = 0.2 s
t = 0.3 s

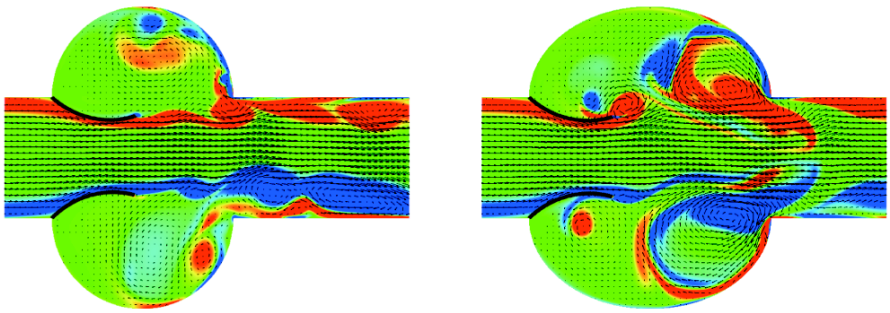

$t = 0.4$ s

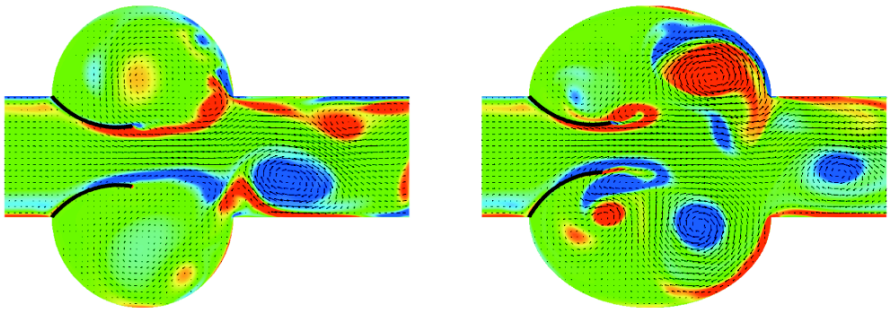

$t = 0.5$ s

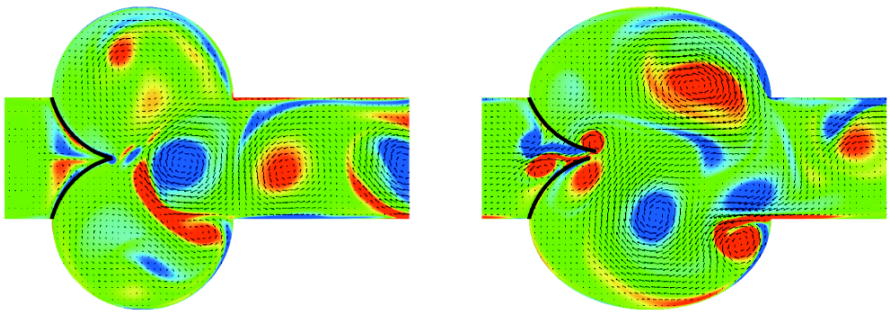

$t = 0.6$ s

Figure 5: Vorticity distribution and velocity vectors on the left for case 1 and right for case 2 in the eighth cardiac cycle at the time interval of 0.1 s.

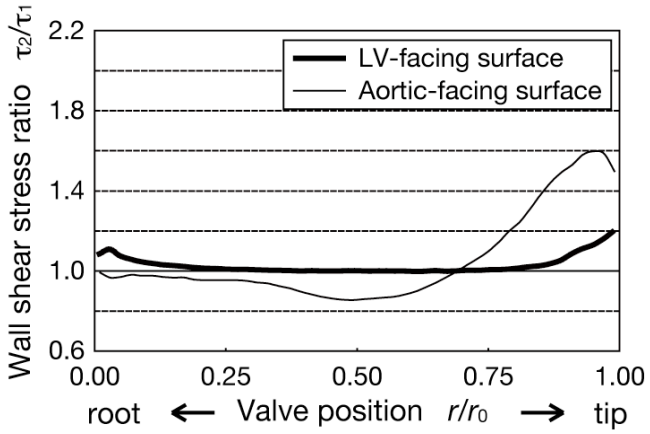

Figure 6: Time averaged WSS ratio distribution on the LV-facing and aortic-facing surfaces.

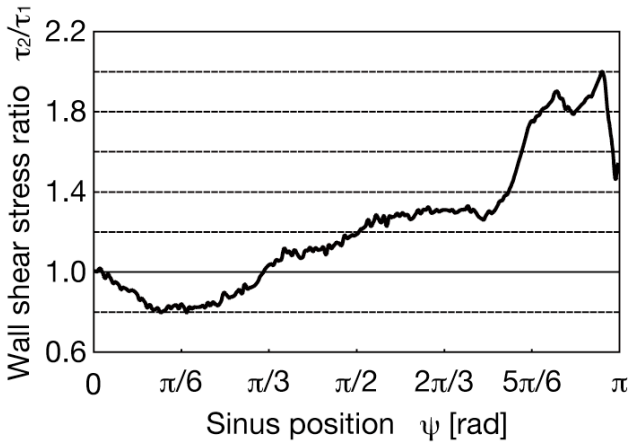

Figure 7: Time averaged WSS ratio distribution on the sinus wall. The sinus position $\psi = 0$ and π rad correspond to proximal and distal edges of the sinus of Valsalva, respectively.

The vortices evolved from the tip of the valve strike on the distal edge of the sinus and spread within the sinus of Valsalva. These vortices affect the WSS distribution of the valves on the tip of the aortic-facing surface and sinus wall near the distal edge. It is well known that the WSS plays a dominant role in determining the physiological mechanics of the endothelial cell in all generations of arteries, and developing vascular pathology such as atherosclerosis [25,26,27]. According to Malek et al. [28], the value of the low shear stress that causes atherosclerosis initiation is 0.4 Pa. Statistically significant inverse relationships between intima-media thickness and local WSS have also been reported [29,30]. It is, therefore, important to investigate the WSS distribution in time and space in order to predict the precise region where cardiovascular disease occurs. Our computational scheme is suitable and promising to reproduce heart valves behavior with neither re-mesh nor re-construction of the model. Incorporating effect of deflection or bending of the heart valves behavior to our computational model will enable us to consider more accurate WSS distribution on the aortic valves in the future work.

REFERENCES

[1] C. Planche, J. Bruniaux, F. Lacour-Gayet, J. Kachaner, J.P. Binet, D. Sidi, E. Villain, Switch operation for transposition of the great arteries in neonates. A study of 120 patients, *Journal of Thoracic Cardiovascular Surgery*, **96**, 354-363, 1988.

[2] R. Pretre, D. Tamisier, P. Bonhoeffer, P. Mauriat, P. Pouard, D. Sidi, P. Vouhe, Results of the arterial switch operation in neonates with transposed great arteries, *Lancet*, **357**, 1826-1830, 2001.

[3] W.G. Williams, B.W. McCrindle, D.A. Ashburn, R.A. Jonas, C. Mavroudis, E.H. Black-stone, Outcomes of 829 neonates with complete transposition of the great arteries 12-17 years after repair, *European Journal of Cardio-thoracic Surgery*, **24**, 1-10, 2003.

[4] C.J. McMahon, W.J. Ravekes, E.O. Smith, S.W. Denfield, R.H. Pignatelli, C.A. Altman, N.A. Ayres, Risk factors for neo-aortic root enlargement and aortic regurgitation following arterial switch operation, *Pediatric Cardiology*, **25**, 329-335, 2004.

[5] J. Losay, A. Touchot, A. Capderou, J.D. Piot, E. Belli, C. Planche, A. Serraf, Aortic valve regurgitation after arterial switch operation for transposition of the great arteries:

Incidence, Risk factors, and Outcome, *Journal of the American College of Cardiology*, **47**, 2057-2062, 2006.

[6] M.F. Swartz, A. Sena, N. Atallah-Yunes, C. Meagher, J.M. Cholette, F. Gensini, G.M. Alfieris, Decreased incidence of supravalvar pulmonary stenosis after arterial switch operation, *Circulation*, **126**, S118-S122, 2012.

[7] K.D.H.M. Vandekerckhove, N.A. Blom, S. Lalezari, D.R. Koolbergen, M.E.B. Rijlaarsdam, M.G. Hazekamp, Long-term follow-up of arterial switch operation with an emphasis on function and dimensions of left ventricle and aorta, *European Journal of Cardio-thoracic Surgery*, **35**, 582-588, 2009.

[8] S. Lalezari, M.G. Hazekamp, M.M. Bartelings, P.H. Schoof, A.C. Gittenberger-De Groot, Pulmonary artery remodeling in transposition of the great arteries: relevance for neoaortic root dilatation, *Journal of Thoracic Cardiovascular Surgery*, **126**, 1053-1060, 2003.

[9] Y.C. Fung, *Biomechanics Circulation*, 2nd edition, New York Berlin Heidelbelg: Springer-Verlag, 42-48, 1997.

[10] T. Fukui, K. Morinishi, Aortic valve oscillation due to vortices in the sinus of Valsalva by virtual flux method, in *Proceedings of the 8th KSME-JSME Thermal and Fluids Engineering Conference*, 2012, 1-4.

[11] T. Fukui, K. Morinishi, Numerical simulation of blood flows in the aorta with aortic valves by virtual flux method, in *Proceedings of the European Congress on Computational Methods in Applied Sciences and Engineering*, 2012, 1-10.

[12] T. Kruger, F. Varnik, D. Raabe, Shear stress in lattice Boltzmann simulations, *Physical Review E*, **79**(046704), 1-14, 2009.

[13] J. Boyd, J. Buick, J.A. Cosgrove, P. Stansell, Application of the lattice Boltzmann model to simulated stenosis growth in a two-dimensional carotid artery, *Physics in Medicine and Biology*, **50**, 4783-4796, 2005.

[14] M. Tamagawa, H. Kaneda, M. Hiramoto, S. Nagahama, Simulation of thrombus formation in shear flows using lattice Boltzmann method, *Artificial Organs*, **33**(8), 604-610, 2009.

[15] L. Axner, A.G. Hoekstra, A. Jeays, P. Lawford, R. Hose, P.M.A. Sloot, Simulations of time harmonic blood flow in the Mesenteric artery: comparing finite element and lattice Boltzmann methods, *Biomedical Engineering Online*, **8**(23), 1-8, 2009.

[16] M. Izham, T. Fukui, K. Morinishi, Application of regularized lattice Boltzmann method for incompressible flow simulation at high Reynolds number and flow with curved boundary, *Journal of Fluid Science and Technology*, **6**(6), 812-821, 2011.

[17] J. Latt, B. Chopard, Lattice Boltzmann method with regularized precollision distribution functions, *Mathematics and Computers in Simulation*, **72**, 165-168, 2006.

[18] I. Tanno, K. Morinishi, K. Matsuno, H. Nishida, Validation of virtual flux method for forced convection flow, *JSME International Journal*, **B49**(4), 1141-1148, 2006.

[19] D. Yu, R. Mei, W. Shyy, A multi-block lattice Boltzmann method for viscous fluid flows, *International Journal for Numerical Method in Fluids*, **39**, 99-120, 2002.

[20] Y. Peng, C. Shu, Y.T. Chew, X.D. Niu, X.Y. Lu, Application of multi-block approach in the immersed boundary-lattice Boltzmann method for viscous fluid flows, *Journal of Computational Physics*, **218**, 460-478, 2006.

[21] P.L. Bhatnagar, E.P. Gross, M. Krook, A model for collision processes in gases: I. Small amplitude processes in changed and neutral one-component system, *Physical Review*, **94**, 511-525, 1954.

[22] J.D. Sterling, S. Chen, Stability analysis of lattice Boltzmann methods, *Journal of Computational Physics*, **123**, 196-206, 1996.

[23] Y.H. Quian, D. d'Humieres, P. Lallemand, Lattice BGK models for Navier-Stokes equation, *Europhysics Letters*, **17**, 479-484, 1992.

[24] R. Mei, D. Yu, W. Shyy, Force evaluation in the lattice Boltzmann method involving curved geometry, *Physical Review E*, **65**(041203), 1-14, 2002.

[25] C.G. Caro, J.M. Fitzgerald, R.C. Schroter, Atheroma and arterial wall shear: observation, correlation and proposal of a shear dependent mass transfer mechanism for atherogenesis, *Proceedings of the Royal Society*, **177**, 109-159, 1971.

[26] D.L. Fry, Certain histological and chemical responses of the vascular interface to acutely induced mechanical stress in the aorta of the dog, *Circulation Research*, **24**, 93-108, 1969.

[27] D.P. Giddens, C.K. Zarins, S. Glagov, The role of fluid mechanics in the localization and detection of atherosclerosis, *Journal of Biomechanical Engineering*, **115**, 588-594, 1993.

[28] A.M. Malek, A.L. Alper, S. Izumo, Hemodynamic shear stress and its role in atherosclerosis, *Journal of the American Medical Association*, **282**, 2035-2042, 1999.

[29] A. Gnasso, C. Carallo, C. Irace, V. Spagnuolo, G. De Novara, P.L. Mattioli, A. Pujia, Association between intima-media thickness and wall shear stress in common carotid arteries in healthy male subjects, *Circulation*, **94**, 3257-3262, 1996.

[30] C. Irac, C. Cortese, E. Fiaschi, C. Carallo, E. Farinaro, A. Gnasso, Wall shear stress is associated with intima-media thickness and carotid atherosclerosis in subjects at low coronary heart disease risk, *Stroke*, **35**, 464-468, 2004.